Kovove Mater. 64 2026 27–34
DOI: 10.31577/km.2026.1.27

Scaling the test to component size: case study for ZhS6K superalloy

Jiří Pavlas[1]*, Ondřej Kovářík[2], Milan Růžička[1], Svatomír Slavík[1]

[1] *Faculty of Mechanical Engineering, Czech Technical University in Prague, Technická 4, 160 00 Prague, Czech Republic*
[2] *Faculty of Nuclear Sciences and Physical Engineering, Czech Technical University in Prague, Břehová 7, 115 19 Prague, Czech Republic*

Received 14 January 2026, received in revised form 4 April 2025, accepted 7 May 2025

Abstract

The purpose of this article is the fatigue crack growth rate and stress-strain characteristic of a nickel superalloys ZhS6K.

The $\mathrm{d}a/\mathrm{d}N(K)$ data from near-threshold to Paris regime and the stress-strain curve were obtained using a new methodology designed for bending small specimens using material extracted directly from the blade.

The Hartmann-Schijve formula was fitted to describe the fatigue crack growth rate data. Failure mechanism was related to the crack propagation rate by help of fractographic analysis. A comparative analysis of the investigated material with the related alloy Inconel 718 was also performed.

The tensile and compression stress-strain behavior, fatigue crack growth rate, and fracture toughness of the ZhS6K nickel superalloy were determined from a single turbine blade, with failure mechanisms examined using scanning electron microscopy. Compared to Inconel 718, ZhS6K offers higher resistance to fatigue crack growth but has significantly lower fracture toughness and stress-strain properties.

The obtained results fill a gap in materials data necessary for the durability and damage tolerance assessment of turbine blades made of ZhS6K alloy.

Although the primary focus is on the fracture behavior of the newly characterized material ZhS6K, the findings contribute to a broader understanding of the fracture mechanics within the entire class of structurally similar materials.

K e y w o r d s: nickel superalloy, ZhS6K, fatigue crack growth rate, small specimen testing, aircraft turbine blade

1. Introduction

ZhS6K is a nickel superalloy used in many aircraft turboshaft, turboprop and jet engines. Recently it also received significant attention as an additively manufactured material [1]. Despite its widespread use, reliable material data is still missing for fracture properties including the crack growth rate. Historically, these material data were substituted by very detailed ground and flight test procedures of the engine parts. One of the most stressed components of an aircraft engine are the blades. These parts are critical, as any structural failure of a single compressor or turbine blade during operation can lead to engine failure, regardless of whether it is a stator or rotor part. Such destruction can cause secondary damage to the fuselage, Then, the aircraft can become inoperative, and this situation can lead to a catastrophic scenario.

Recently, several military training and rescue air accidents have occurred involving compressor and turbine blades damage and subsequent destruction of the entire engine, resulting in an emergency landing. Clear causes of some accidents have not yet been found. However, during regular inspections using Non-destructive testing (NDT) methods, damage of the protective coating and sometimes also of the substrate material, including the formation of fatigue microcracks, was observed on the blades.

*Corresponding author: e-mail address: jiri.pavlas@fs.cvut.cz

Table 1. Chemical composition of nickel alloy ZhS6K (wt.%) [10]

Ni	Cr	Co	Mo	W	Al	Ti	Fe	Mn	Si	C	B	Zr
Balance	10.5	5.2	4.1	4.7	5.5	2.8	1.8	0.4	0.4	0.15	0.035	0.04

Degradation effects of nickel alloys are described in [2–5]. Known damage of blades made of ZhS6K from operated engines was investigated in the subsonic jet engine DV-2 [6], the helicopter turboshaft engine TV3-117 [7] and the supersonic jet engine RD-33 [8]. Also degradation of the protective coating covering the substrate material ZhS6K has been identified and analysed [9–11]. These research papers demonstrate the relation between the protective coating and substrate material. However, these references were not addressing the fatigue phenomena of the substrate material.

It is extremely difficult to test, predict and detect these potential fatigue cracks during the regular general overhaul procedure or even between the flights. The ability to identify and assess the level of degradation and detect the hidden fatigue cracks is essential for ensuring the safety and airworthiness of turboshaft engines. The complexity of air accident investigation is shown in [12]. A general overview and summary concerning blade damages are reviewed in [13] and [14].

Ground testing is limited by the fact that each disassembly process is very expensive and the original settings change during repeated assembly. Natural boundary conditions (environment, pilot response, weight) cannot be taken into account. Flight testing with known fatigue damage is unfortunately almost impossible. Therefore, the microstructure and material degradation processes in cast of ZhS6K were brought into focus.

This paper aims to collect the necessary data for fatigue life assessment and accident analysis using unique resonance bending testing methodology of small specimens.

In this research, a stress-strain test and a series of fatigue tests were performed. The crack growth properties of the material were analysed. Additionally, the fracture surface morphology at different crack growth rates was also investigated.

2. Materials and methods

This chapter describes an experimental program focused on an obtaining mechanical and fracture properties of the ZhS6K alloy taken directly from a manufactured component. A compressor stator blade from the jet engine M701 was chosen for the investigation. Although this type of engine is no longer used very much, ZhS6K material is used very widely in turboshaft and jet engines.

Certification specification and aviation standards EASA [15] or FAA [16] do not contain specific required material testing procedures. New testing approaches using the rotational specimen were designed [17] and [18]. Unfortunately, the effect of production from a real blade is missing. So, we used a testing methodology developed at Faculty of Nuclear Sciences and Physical Engineering, Czech Technical University in Prague [19]. This methodology was implemented to study the Fatigue Crack Growth Rate (FCGR), fracture toughness and stress-strain behavior [20]. The use of small bending test specimens cut from the blade enabled to test small amounts of materials that can potentially be obtained from parts with specific service history. The experiments were performed in ambient air at room temperature.

2.1. Material composition

ZhS6K is a Nickel superalloy with low Fe content and high Cr, W, Mo, and Co content. The main elements supporting the formation of the γ' phase are Al and Ti. The blade material is coarse-grained with equiaxial grains. Temperature of liquid at casting in vacuum to form is 1500–1600 ℃. Working temperature up to 800–1050 ℃. The material composition of the samples is defined in Table 1. The protective Aluminum layer usually covers ZhS6K material against the effects of high-temperature corrosion caused by high temperature and exhaust gases during operation. The thickness of the layer ranges from 0.02 to 0.05 mm. This protective layer is not the subject of this investigation.

A conventionally manufactured, wrought Inconel 718 in the form of a 12 mm thick bar (Bibus Metals AG, Fehraltorf, Switzerland) was used as a reference. The material was subjected to standard heat-treatment (1000 ℃ for 30 minutes + in a protective atmosphere, 720 ℃/8 h + 620 ℃/18 h aging).

2.2. The test specimens

Material from never operated turbine blade was tested. Six miniature samples ($4 \times 3 \times 32\,\mathrm{mm}^3$) were cut by electric discharge machining as shown Fig. 1. Then the artificial notch was cut using diamond blade [19] as shows Fig. 2. The depth of the notch was 0.4 mm, and width was 0.15 mm. Specimens 1, 3, and 4, according to Fig. 1 were notched, remaining specimens were used to obtain stress-strain curves and as spare parts.

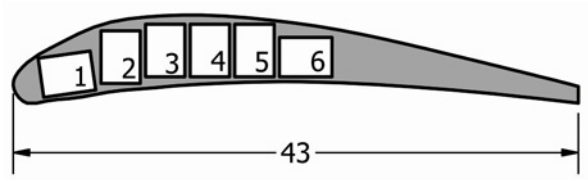

Fig. 1. The test specimen – turbine blade and the cut plan.

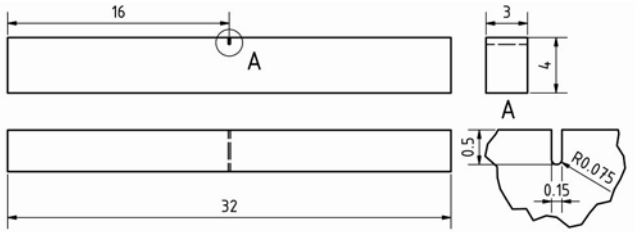

Fig. 2. The sample with the initial crack cut from the specimen.

2.3. Mechanical properties

Stress-strain properties were measured for specimen 2. Bending setup instrumented by Digital Image Correlation (DIC) system based on the *Ncorr software* [21] was used. The load/strain data were then evaluated by the method of Herbert [19–23] to obtain stress-strain curves in tension and compression.

2.4. Methodology

The used testing device [19] is shown in Fig. 3. It loads the specimen in pure bending with stress ratio $R \sim -1$ and loading frequency of around 300 Hz. During the test, the fatigue crack was initiated first by stepwise increasing load with a holding period of 500,000 cycles. Once the crack was initiated, different approaches were used for the testing. For specimen 1, the constant amplitude was used up to 1 mm crack length, followed by K controlled load reduction.

For other specimens, the crack grew in the rate-control mode [19] to reach crack length $a = 1$ mm at 5×10^{-11} m cycle^{-1}.

Then the fatigue crack growth rate was exponentially increased to 10^{-6} m cycle^{-1} at 2 mm crack length for specimen 4. For specimen 3, the load increase K-control mode of the ASTM E647 [24] standard was used.

After the fatigue crack growth rate test, the specimen was ruptured during fracture toughness test according to ASTM E1820 [25] standard. The crack length was measured by unloading compliance instrumented by a Linear Variable Differential Transformer (LVDT) sensor. After the fracture toughness test, the fracture surfaces of the test specimens were examined using a JEOL JSM IT-500HR Scanning Electron Microscope (SEM).

Microstructure was observed on metallographically polished surface using JEOL JSM 5510-LV SEM (JEOL, Osaka, Japan) in backscattered electron mode. Chemical composition was measured by energy dispersive X-ray analysis (EDX) using IXRF 500 system (IXRF, Inc. Austin, TX, USA) in the same SEM.

3. Results and discussion

In this chapter, selected experimental results from the stress-strain test, fatigue crack growth rate and fracture toughness test conducted on ZhS6K specimens are presented and related to the findings of fracture surface analysis.

3.1. Microstructure

The metallography of the investigated alloy is in Fig. 4. The alloy showed typical dendritic structure with substructure formed by coarse γ', similar to that presented in [26]. Interdendritic areas contained white elongated particles (denoted Ti in Fig. 4) with in-

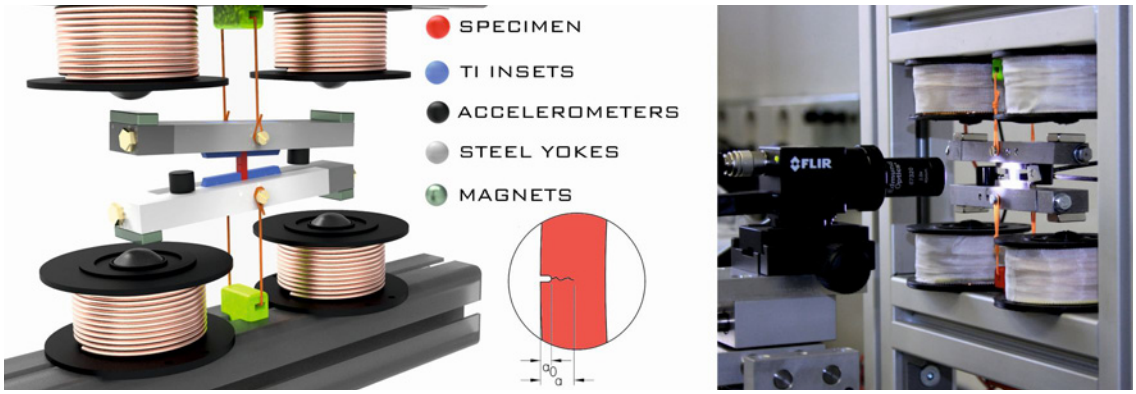

Fig. 3. The fatigue crack growth rate testing device.

Table 2. Nominal and measured chemical composition of nickel alloy ZhS6K obtained by EDX (wt.%)

	Ni	Cr	Co	Mo	W	Al	Ti	Fe	Mn	Si	C	B	Zr
Nominal	Balance	10.5	5.2	4.1	4.7	5.5	2.8	1.8	0.4	0.4	0.15	0.035	0.04
Average		11.3	4.5	5	4.4	3.11	2.9	0.5	0.1	0.03	–	–	–
Ni		4.4	2.8	2.2	1	4.3	6.3	0.2	0.03	0.02	–	–	–
Ti		2.41	0.31	25.9	32.1	0.1	34.73	0.21	0.2	0.14	–	–	–

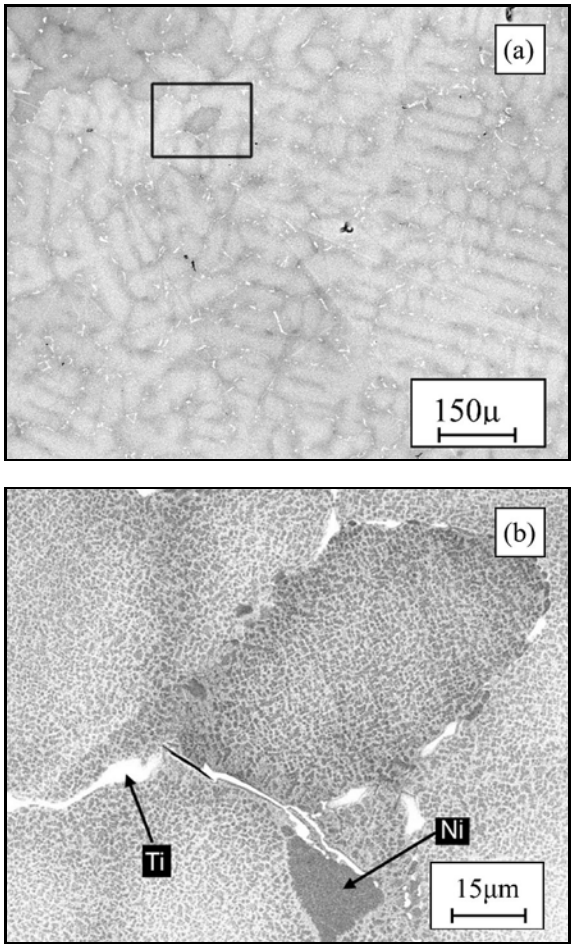

Fig. 4. Microstructure of the investigated ZhS6K alloy. Box indicates detailed location, Ti and Ni indicate Ti rich and Ni rich areas.

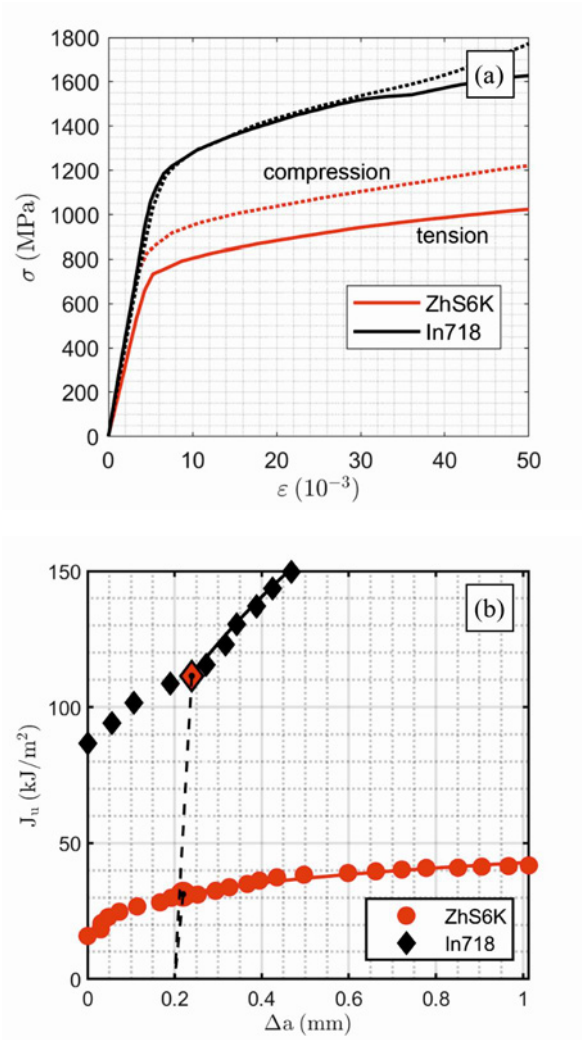

Fig. 5. The stress-strain curves in tension, obtained from the bending test (a) and R-curve from fracture toughness measurement (b).

creased concentration of the alloying elements (see Table 2). These elongated particles may correspond to carbides particles described in [26] or to intermetallic precipitates. Darker particles (denoted Ni in Fig. 4 and Table 2) on the other hand contain lower than nominal concentration of the alloying elements. One exception is Ti which is present in twice the nominal concentration in these darker areas.

3.2. Stress-strain test

Sample 2 was subjected to the bending test using the Herbert method implemented according to [27]. The resulting stress-strain curves in tension and compression are shown in Fig. 5 and compared with reference Inconel 718 material [28]. The significant difference in compression and tensile behavior may be a material property or may be caused by the inhomogeneity of the material. The difference is quantified by the mechanical properties in Table 3.

Table 3. Mechanical properties in tension and compression (subscript t and c), elastic modulus E and yield strength YS

Sample	E_t (GPa)	E_c (GPa)	YS_t (MPa)	YS_c (MPa)
ZhS6K	160	214	757	877
In718	219	218	1199	1260

Table 4. Coefficients of the Hartmann-Schijve formula and mechanical properties in tension-elastic modulus E_t and yield strength YS_t

Sample	ΔK_{th} (MPa m$^{0.5}$)	ΔK_{thr} (MPa m$^{0.5}$)	A (MPa m$^{0.5}$)	D (10^{-11})	p
1 (LR)	9.07	7.53	65		
3 (KC)	8.84	7.3	65	3.37	2.15
4 (rate)	10.11	8.59	65		
In718	6.7	5.5	145	6.28	2.25

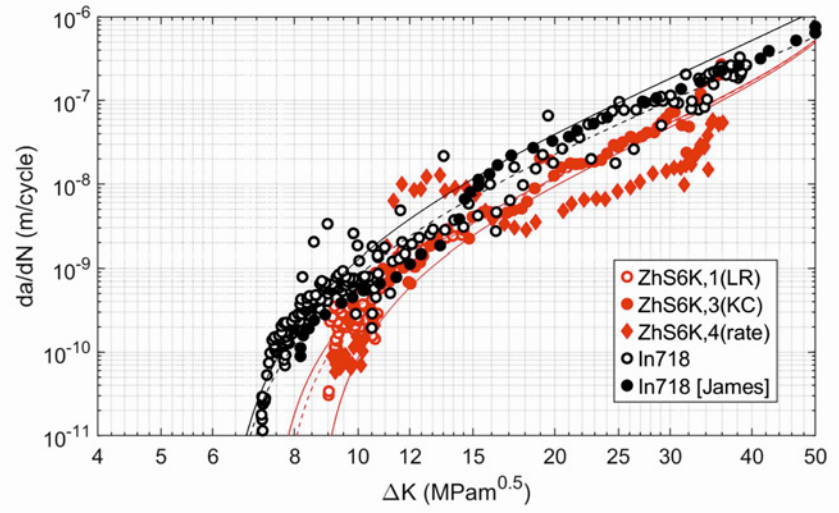

Fig. 6. The fatigue crack growth rate curves at $R \sim -1$ at room temperature: LR – load reduction, KC – K-control, rate – rate control. Reference In718 data were obtained by the same method. Another reference is from [28] at $R = 0.1$.

3.3. Fatigue crack growth rate and fracture toughness test

The obtained da/dN vs. K_{max} data and corresponding parameters of the Hartmann-Schijve [29] formula are summarized Fig. 6 and Table 4. The Hartmann-Schijve formula relates fatigue crack propagation rate da/dN to driving forces ΔK and K_{max} as:

$$da/dN = D(\Delta K - \Delta K_{thr})^p/(1 - K_{max}/A)^{p/2}, \quad (1)$$

where ΔK_{thr} is the stress intensity factor range at fatigue crack growth rate threshold (note the different threshold ΔK_{th} corresponding to $da/dN = 10^{-10}$ m cycle^{-1} by ASTM E647). Following the ASTM E647 recommendation for the used $R \sim -1$, it is assumed that $\Delta K = K_{max}$. It is also assumed that the dynamic fracture toughness A can be approximated by the measured fracture toughness K_{IC}. The detailed description of fitting the formula to experimental data is in [20].

The coarse microstructure of ZhS6K causes significant variability of the FCGR curves, over the whole tested range. The H-S however indicate higher fatigue crack growth threshold and lower propagation rate in Paris regime compared to the reference Inconel 718.

It may be interesting to mention that the ZhS6K requires ΔK approximately 20 % higher than the reference fully heat-treated Inconel 718 commonly applied to turbine blades in aircraft power units. Its fracture toughness only reaches about 50 % of In 718. The In718 tested using the same method in rate control are also included. These data are comparable to standard CT tests at $R = 0.1$ taken from [28].

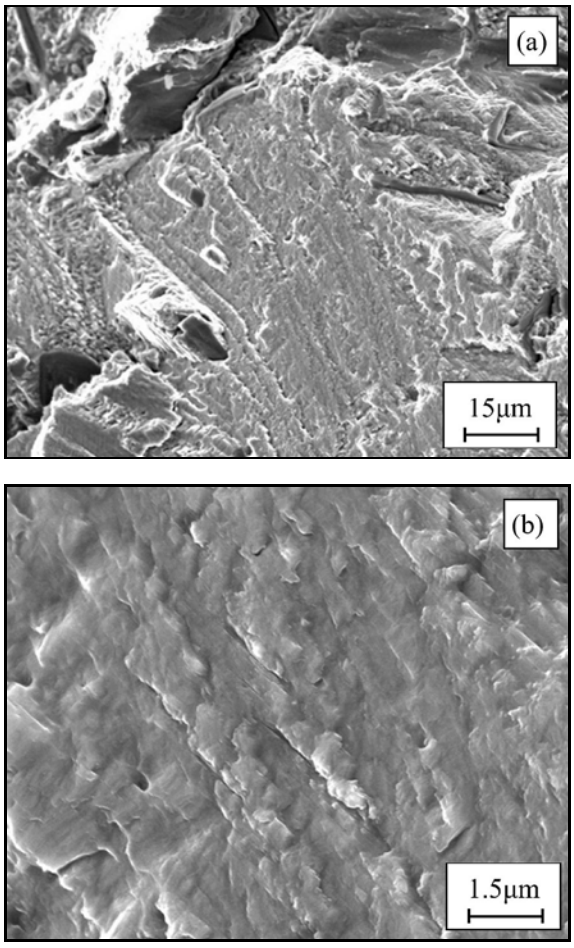

Fig. 7. Fatigue surface at $K \sim 35$ MPa m$^{0.5}$.

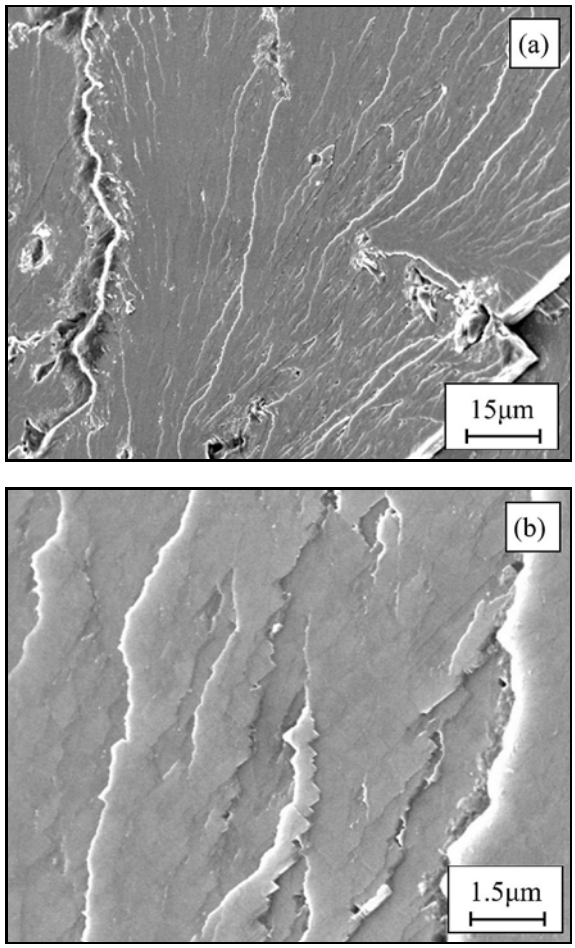

Fig. 8. Fatigue surface at $K \sim 20$ MPa m$^{0.5}$.

3.4. Fracture surface analysis

Sample 4 from Fig. 1 was subjected to fractographic analysis. Fracture surfaces corresponding to near threshold, Paris and high load crack propagation regimes characterized by $K_{\max}$ of 35 MPa m$^{0.5}$ (Fig. 7), 20 MPa m$^{0.5}$ (Fig. 8), and 10 MPa m$^{0.5}$ (Fig. 9). The fractures are rugged, following the crys-

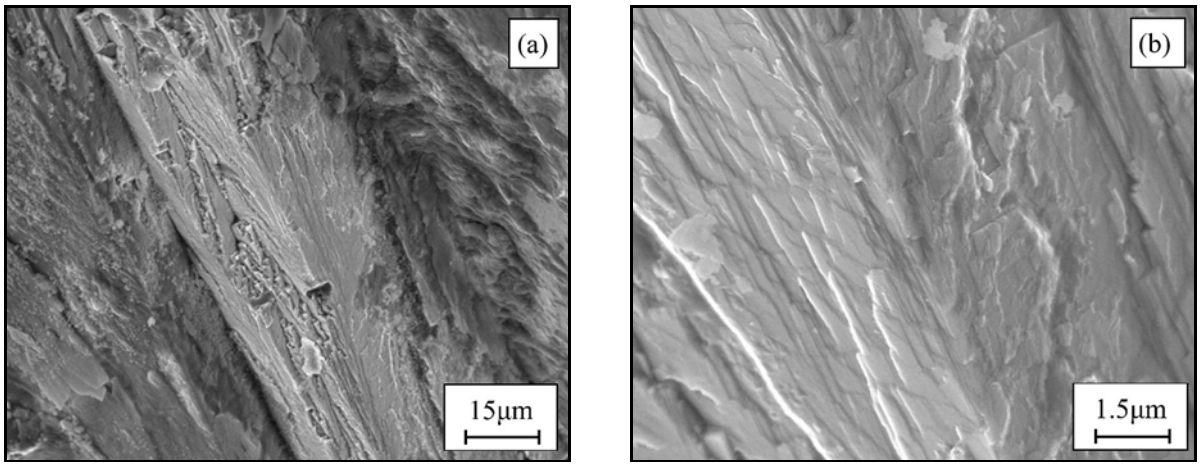

Fig. 9. Fatigue surface at $K \sim 10$ MPa m$^{0.5}$.

tal anisotropy of large areas with the same crystal orientation. At high loads at the end of the fatigue test, cracks propagate by the striation mechanism.

4. Conclusion

The stress-strain relation in tension and compression, fatigue crack growth rate and fracture toughness and of ZhS6K Ni superalloy were obtained from a single turbine blade.

SEM was employed to investigate the failure mechanisms. Compared with Inconel 718 alloy, ZhS6K shows around 20 % higher fatigue crack growth resistance, but at the same time, its fracture toughness and stress-strain properties are significantly lower. These findings provide valuable insights into the similarities between these alloys, informing future material selection and development for high-stress applications.

The performed testing demonstrates the capabilities of the used methodology to obtain material data very efficiently from a small amount of material. Despite its present limitations to room temperature testing, it can support failure analysis by providing actual part/batch material engineering data.

The next steps will focus on terminal phase of the failure process, i.e. to the investigation of material fracture toughness at elevated temperature. The main research goal of these activities is a detailed description of ZhS6K material and increasing the operational safety of actively used aircraft engines with this nickel alloy.

Acknowledgements

This study was supported by the Czech Technical University in Prague, Faculty of Mechanical Engineering. The project FerrMion of the Ministry of Education, Youth, and Sports, Czech Republic, co-funded by the European Union (CZ.02.01.01/00/22_008/0004591) and the project SGS24/147/OHK4/3T/14SGS of the Grant Agency of the Czech Technical University are gratefully acknowledged.

References

[1] E. A. Lukina, K. O. Bazaleeva, N. V. Petrushin, I. A. Treninkov, E. V. Tsvetkova, Effect of the selective laser melting parameters on the structure–phase state of a ZhS6K VI nickel superalloy, Russ. Metall. (2017) 594–600. https://doi.org/10.1134/S0036029517070102

[2] J. Błachnio, J. Spychała, D. Zasada, Analysis of structural changes in a gas turbine blade as a result of high temperature and stress, Eng. Fail. Anal. 127 (2021) 105554. https://doi.org/10.1016/j.engfailanal.2021.105554

[3] G. M. Han, J. J. Yu, X. F. Sun, Z. Q. Hu, Thermo-mechanical fatigue behavior of a single crystal nickel-based superalloy, Mater Sci Eng A. 528 (2011) 6217–6224. https://doi.org/10.1016/j.msea.2011.04.083

[4] J. Kanesund, H. Brodin, S. Johansson, Hot corrosion influence on deformation and damage mechanisms in turbine blades made of IN-792 during service, Engineering Failure Analysis 110 (2020) 104388. https://doi.org/10.1016/j.engfailanal.2020.104388

[5] A. I. Rybnikov, L. B. Getsov, A. A. Tchizhik, I. S. Malashenko, A. S. Osyka, Service life of heat-resistant alloys with protective coatings in thermocyclic loading, Surface and Coatings Technology 78 (1996) 103–112. https://doi.org/10.1016/0257-8972(94)02397-2

[6] J. Belan, L. Kucharikova, A. Vasko, E. Tillova, The influence of high temperature on DV-2 jet engine Ni-based superalloy turbine blade degradation, Materials Today: Procceeding 4 (2017) 5743–5748. https://doi.org/10.1016/j.matpr.2017.06.039

[7] J. Pavlas, M. Růžička, S. Slavík, Surface fatigue microcracks in turbocompressor blades of a turboshaft engine, Applied and computational Mechanics 19 (2025) 87–96. https://doi.org/10.24132/acm.2025.960

[8] J. Čerňan, M. Janovec, M. Hocko, M. Cúttová, Damages of RD-33 engine gas turbine and their causes, Transportation Research Procedia 35 (2018) 200–208. https://doi.org/10.1016/j.trpro.2018.12.028

[9] J. Belan, Quantitative Evaluation of Alitize Coating on ŽS6K Ni-Base Superalloy, Materials Science Forum 782 (2014) 578–583. https://doi.org/10.4028/www.scientific.net/MSF.782.578

[10] B. Chmiela, M. Kianicová, M. Sozańska, L. Swadźba, Degradation of Si-Al aluminide coating after service of turbine blades made of ZhS6K superalloy, IOP Conference Series: Materials Science and Engineering 35 (2012) 012010. https://doi.org/10.1088/1757-899X/35/1/012010

[11] L. Swadźba, A. Maciejny, B. Formanek, J. Biedroń, Microstructure and resistance to cracking of modified Al-Si and Al-Cr diffusion coatings on ŻS6K nickel-based superalloys, Surface and Coatings Technology 54–55 (1992) 84–90. https://doi.org/10.1016/S0257-8972(09)90032-9

[12] V. Infante, M. Freitas, Failure analysis of compressor blades of a helicopter engine, Engineering Failure Analysis 104 (2019) 67–74. https://doi.org/10.1016/j.engfailanal.2019.05.024

[13] P. Yang, W. Yue, J. Li, G. Bin, Ch. Li, Review of damage mechanism and protection of aero-engine blades based on impact properties, Engineering Failure Analysis 140 (2022) 106570. https://doi.org/10.1016/j.engfailanal.2022.106570

[14] T. S. Chowdhury, F. T. Mohsin, M. M. Tonni, M. N. H. Mitta, M. M. Ehsan, A critical review on gas turbine cooling performance and failure analysis of turbine blades, International Journal of Thermofluids 18 (2023) 100329. https://doi.org/10.1016/j.ijft.2023.100329

[15] European Union Aviation Safety Agency. 2025. Certification Specifications and Acceptable Means of Compliance for Engines (CS-E), Amendment 8.

[16] Federal Aviation Administration. 2025. Part 33—Airworthiness Standards: Aircraft Engines.

[17] M. Bartošák, M. Horváth, M., Gálíková, M. Slaný, I., Šulák, High-temperature low-cycle fatigue and

fatigue–creep behaviour of Inconel 718 superalloy: Damage and deformation mechanisms, International Journal of Fatigue 186 (2024) 108369. https://doi.org/10.1016/j.ijfatigue.2024.108369

[18] G.-C. Pan, B.-W. Zou, W. Li, C.-X. Chen, W.-W. Zhao, G.-Q. Wang, M.-S. Chen, Y.-C. Lin, An LSTM-PSO model for forecasting the flow behavior of a Ni-based superalloy during hot deformation, Kovove Mater. 62 (2024) 53–64. https://doi.org/10.31577/km.2024.5.285

[19] J. Cizek, O. Kovarik, J. Cupera, J. Kondas, T. Bajer, F. Siska, M. Janovska, H. Seiner, Measurement of mechanical and fatigue properties using unified, simple-geometry specimens: Cold spray additively manufactured pure metals, Surface and Coatings Technology 412 (2021) 126929. https://doi.org/10.1016/j.surfcoat.2021.126929

[20] O. Kovarik, J. Cizek, J. Klecka, Fatigue Crack growth rate description of RF-plasma-sprayed refractory metals and alloys, Materials 16 (2023) 1713. https://doi.org/10.3390/ma16041713

[21] J. Blaber, A. Adair, A. Antoniou, Ncorr: Open-Source 2D Digital Image Correlation Matlab Software, Experimental mechanics 55 (2015) 1105–1122. https://doi.org/10.1007/s11340-015-0009-1

[22] H. Herbert, On the relationship between the bending elasticity of cast iron and its tensile and compressive elasticity. Forschungsarbeiten auf dem Gebiete des Ingenieurwesens, Springer, Berlin, Heidelberg 59 (1910) 39–81. (in German) https://doi.org/10.1007/978-3-662-02218-4_2

[23] R. A. Mayville, I. Finnie, Uniaxial stress-strain curves from a bending test, Experimental Mechanics 22 (1982) 197–201. https://doi.org/10.1007/BF02326357

[24] ASTM E-647 Standard Test Method for Measurement of Fatigue Crack Growth Rates

[25] ASTM E-1820 Standard Test Method for Measurement of Fracture Toughness

[26] J. Belan, L. Kuchariková, E. Tillová, M. Matvija, M. Uhríčik, The hardness evolution of cast and the high-cycle fatigue life change of wrought Ni-base superalloys after additional heat treatment, Materials 14 (2021) 7427. https://doi.org/10.3390/ma14237427

[27] H. Kato, Y. Tottori, K. Sasaki, Four-point bending test of determining stress-strain curves asymmetric between tension and compression, Experimental Mechanics 54 (2014) 489–492. https://doi.org/10.1007/s11340-013-9791-9

[28] L. A. James, Fatigue crack propagation in Alloy 718: A review. Superalloy 718: Metallurgy and Applications, The Minerals, Metals and Materials Society (1989) 499–515. https://doi.org/10.7449/1989/Superalloys_1989_499_515

[29] A. Hartman, J. Schijve, The effects of environment and load frequency on the crack propagation law for macro fatigue crack growth in aluminium alloys, Engineering Fracture Mechanics 1 (1970) 615–631. https://doi.org/10.1016/0013-7944(70)90003-2